ASSEMBLY OF GAP JUNCTIONS DURING AMPHIBIAN NEURULATION

ROBERT S. DECKER and DANIEL S. FRIEND

From the Department of Pathology, University of California, San Francisco, California 94143. Dr. Decker's present address is the Department of Cell Biology, University of Texas, Southwestern Medical School, Dallas, Texas 75235.

ABSTRACT

Sequential thin-section, tracer (K-pyroantimonate, lanthanum, ruthenium red, and horseradish peroxidase), and freeze-fracture studies were conducted on embryos and larvae of *Rana pipiens* to determine the steps involved in gap junction assembly during neurulation. The zonulae occludentes, which join contiguous neuroepithelial cells, fragment into solitary domains as the neural groove deepens. These plaque-like contacts also become permeable to a variety of tracers at this juncture. Where the ridges of these domains intersect, numerous 85-Å participles apparently pile up against tight junctional remnants, creating arrays recognizable as gap junctions. With neural fold closure, the remaining tight junctional elements disappear and are replaced by macular gap junctions. Well below the junctional complex, gap junctions form independent of any visible, preexisting structure. Small, variegated clusters, containing 4–30 particles located in flat, particle-free regions, characterize this area. The number of particles within these arrays increases and they subsequently blend together into a polygonally packed aggregate resembling a gap junction. The assembly process in both apical and basal regions conforms with the concept of translational movement of particles within a fluid plasma membrane.

INTRODUCTION

The presence of intercellular contacts appears to be prerequisite for such diverse phenomena as metabolic cooperation (3, 28), electrotonic coupling (5, 15, 43), and perhaps contact inhibition as well (1, 45, 75). During embryogenesis, electrotonic coupling seems to correlate with the genesis of low-resistance membrane rather than with the surface barrier of high resistance which encases some embryos (6, 7, 34). Likewise, pathways of low-resistance coupling and the differentiation of cellular contacts, specifically those which represent forms of membrane fusion, appear simultaneously (5). Several investigators first implicated septate and gap junctions between invertebrate cells (26, 27, 33, 50, 54, 55, 72) and tight and gap junctions between vertebrate cells (11, 16, 22, 30, 46, 47, 73, 81) as avenues of such coupling. However, combined fine-structural and electrophysiological studies on the crayfish segmental axon presented compelling evidence that the gap junction is the site of low-resistance coupling (2, 5, 52–55). Other workers (28, 36, 64) have also found gap junctions and ionic coupling coexisting in cell cultures, affording further solid support for this association.

The use of tracer and freeze-fracturing techniques confirms that the gap junction (46, 66)

exhibits a 2 to 4-nm gap between cell membranes and is comprised of 8.5-nm, polygonally packed subunits (4, 11, 22, 30, 46, 47, 51, 63). Freeze fracture further reveals that the junction assumes a variety of configurations (22, 62, 66) and cannot always be identified by thin sectioning alone (22, 65).

Surprisingly, this ubiquitous junction has been observed during embryogenesis only rarely (7, 15, 38, 42, 65), whereas focal (65, 78) and truly occluding tight junctions (17, 42, 45, 65) and septate desmosomes (25, 29) have been extensively described. Although the temporal appearance of some junctional elements (gap junction and zonula occludens) has been established (17, 42), little information has been published on the construction of these junctional components (25) and their interrelationships. The present study delineates a dual mode of assembly of gap junctions during amphibian neurulation and the changing patterns of epithelial permeability to lanthanum, potassium (K−) pyroantimonate, ruthenium red, and horseradish peroxidase.

MATERIALS AND METHODS

Materials

Embryonic *Rana pipiens* were obtained by artificially induced ovulation and reared in aquaria of aerated tap water maintained at 18 ± 1°C. In this investigation emphasis was placed on the examination of all phases of neurulation (69); therefore, embryos were selected at 2.5-h intervals beginning with late gastrulae (stage 12, 42 h of age) and concluding with neural tube embryos (stage 16, 72 h of age). At each of the 12 interims, the presumptive medulla oblongata was removed and prepared for thin sectioning or freeze cleaving. In each instance, only the neural groove and its lateral walls or the ventral half of the neural tube was utilized so that we could reliably compare all developmental stages.

Reagents

The following reagents, enzymes, and substrates were utilized: horseradish peroxidase (type II), and 3,3'-diaminobenzidine tetrahydrochloride (Sigma Chemical Co., St. Louis, Mo.); lanthanum nitrate and K-pyroantimonate (Fisher Scientific Co., Fair Lawn, N. J.); glutaraldehyde; paraformaldehyde; acrolein (Polysciences, Inc., Warrington, Pa.); and ruthenium red (Johnson, Matthey and Co., New York).

Methods

PREPARATION OF EMBRYONIC TISSUE FOR ELECTRON MICROSCOPY: After the removal of the jelly envelopes with fine watchmaker's forceps, embryos of all developmental stages (69) were preserved *in situ* in a modification of Kalt's and Tandler's (39) trialdehyde fixative, consisting of 2.5% glutaraldehyde, 1.5% formaldehyde (prepared from paraformaldehyde), 1% acrolein buffered to pH 7.4 with 0.1 M sodium cacodylate, and 0.25 mM $CaCl_2$. Occasionally, 2.5% dimethylsulfoxide (DMSO) was added to facilitate penetration of the fixative. After 5 min of fixation, the embryos were removed and placed in fresh fixative for 4–8 h at room temperature. In some experiments, $CaCl_2$ was replaced by 1% K-pyroantimonate in the fixative to improve the staining of cell junctions (22). The embryos were washed overnight in several changes of 0.1 M cacodylate buffer (pH 7.4) with 7% sucrose, followed by 1-h postfixation at 4°C in 1% OsO_4 buffered to pH 7.4 with acetate-Veronal plus 5% sucrose. Neural plates, grooves, and tubes were then rinsed for 1 h in buffered 0.5% uranyl acetate, rapidly dehydrated in ethanol and propylene oxide, and embedded in Epon 812.

PREPARATION OF LARVAL TISSUE FOR ELECTRON MICROSCOPY: Larvae were fixed by vascular perfusion with 2% glutaraldehyde, 1% formaldehyde and 0.5% acrolein buffered in 0.1 M cacodylate, pH 7.4. After 2–3 h, the medulla oblongata was removed, diced, and placed in fresh fixative for 4–6 h. The tissue slices were then processed as outlined in the previous section.

LIGHT AND ELECTRON MICROSCOPE PROCEDURES: Silver-to-grey thin sections were cut with DuPont diamond knives on a Porter-Blum Sorvall MT-2 ultramicrotome (Ivan Sorvall, Inc., Newtown, Conn.) They were picked up on carbon-stabilized and Formvar-coated 200-mesh grids, stained with 5% aqueous uranyl acetate followed by alkaline lead, and viewed with a Siemens Ia electron microscope at 80 Kv. For light microscopy, 1-μm sections were cut with glass knives and stained with toluidine blue in borax.

TRACER TECHNIQUES: (*a*) Lanthanum. For embryonic and larval tissue, equal parts of fixative and an aqueous 3% solution of lanthanum nitrate (63) were mixed and then used as described above. Colloidal lanthanum was not utilized during washing, postfixation, or dehydration. (*b*) K-pyroantimonate. Embryos and larvae were prepared with specific fixatives containing 5% K-pyroantimonate, pH 7.2, without $CaCl_2$. The pyroantimonate fixative was prepared according to the procedure of Friend and Gilula (22), and fixation was continued for 4–6 h. Subsequent processing was the same as outlined above. (*c*) Horseradish peroxidase. Dejellied embryos were placed in Holtfreter's solution containing 1% horseradish peroxidase for 15–30 min at room temperature before fixation in Karnovsky's glutaraldehyde-paraformaldehyde. For larvae, 1% horseradish peroxidase was dissolved in amphibian Ringer's and then perfused for 1–3 min before Karnovsky's fixative was employed. After brief (1–2 h) fixation, tissue was dissected free, washed overnight in 0.1 M cacodylate buffer (pH 7.4) plus 7% sucrose, and 35-μm tissue sections were

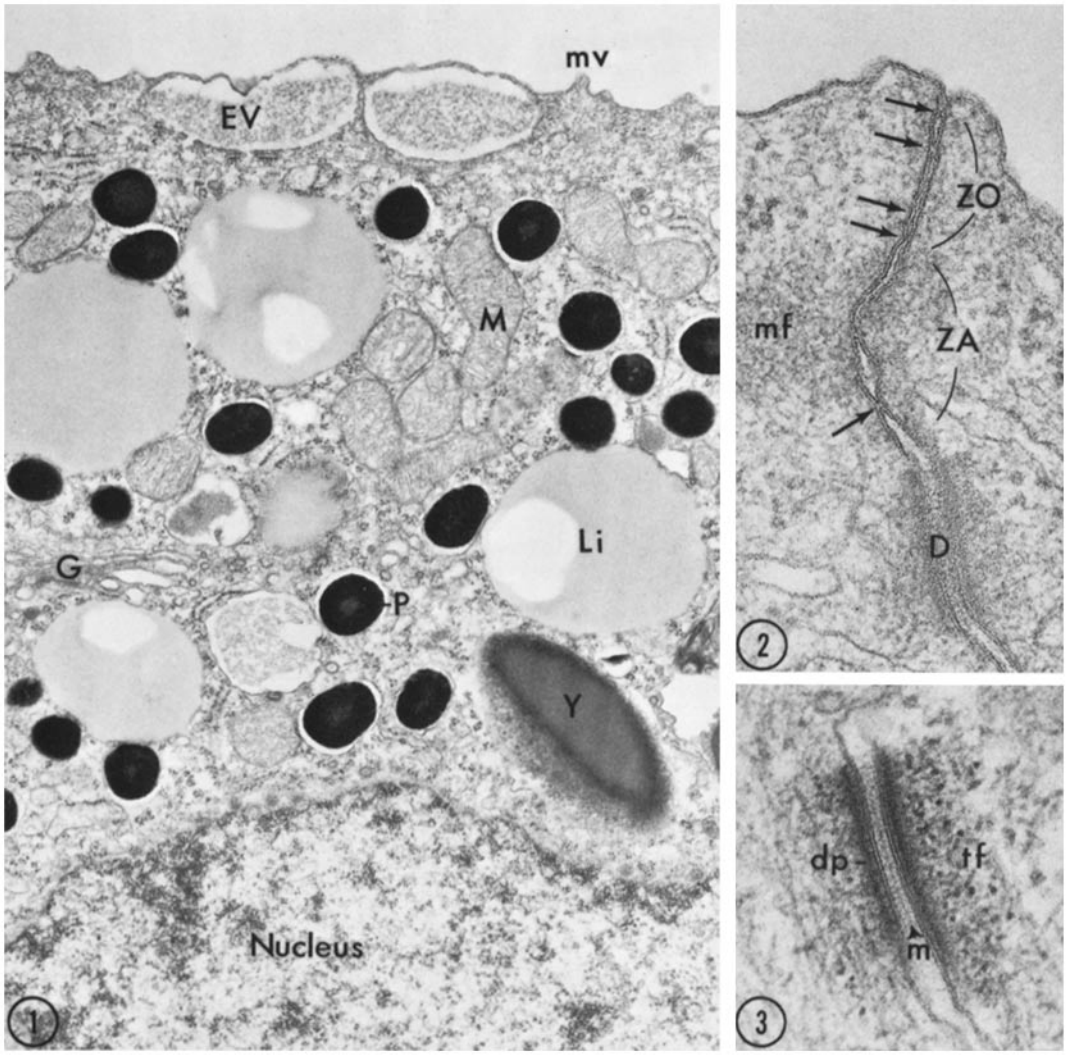

FIGURE 1 Prospective neuroepithelial cells from preneurulating embryos (stage 12). These cells are characterized by widely dispersed lipid inclusions (*Li*), pigment granules (*P*), yolk platelets (*Y*), moderately abundant mitochondria (*M*), and small paranuclear Golgi complexes (*G*). Epidermal vesicles (*EV*) reside just below the embryonic, smoothly contoured surface with its few microvilli (*mv*). × 16,000.

FIGURES 2 and 3 Components of the junctional complex which joins contiguous cells such as the one in Fig. 1. The first element, the zonula occludens (*ZO*), consists of a series of pentalaminar membrane fusions (arrows). Below the *ZO* is the zonula adherens (*ZA*) with microfilaments (*mf*) apparently attached. Occasionally, punctate membrane fusions (arrow) are found in this area. The desmosome (*D*) is the basal element in the complex. Fig. 3: An adjacent thin section of the desmosome in Fig. 2. Note the dense plaques (*dp*), tonofilaments (*tf*), the median line (*m*) typical of anuran desmosomes. Fig. 2, × 78,000; Fig. 3, × 72,000.

then processed with Karnovsky's diaminobenzidine as substrate. (*d*) Ruthenium red. Embryos were immersed in the trialdehyde fixative containing 500 ppm of ruthenium red (44) for 4–6 h, followed by an overnight rinse in 0.1 M cacodylate buffer with the same concentration of tracer. For larvae, the ruthenium red (500 ppm) was placed in the perfusate. No tracer was utilized during postfixation.

FREEZE FRACTURING: For freeze fracturing, small pieces of briefly fixed (15–30 min) embryonic or larval tissue were immersed in 20% glycerol buffered in 0.1 M cacodylate (pH 7.4) at 4°C for a minimum of 4 h. This tissue was mounted on small cardboard disks and oriented so that a transverse cleavage could be achieved. The disks were then rapidly frozen in liquid Freon 22, cooled in liquid nitrogen, and fractured and shadowed in a Balzers apparatus (BA360M, Balzers High Vacuum Corp., Santa Ana, Calif.) according to the technique of Moor and Muhlethaler (48) and Branton (8).

TERMINOLOGY: The terminology used in this study is that employed by Friend and Gilula (22).

RESULTS

Cell Junctions in Prospective Neural Ectoderm

AMPHIBIAN JUNCTIONAL COMPLEX: Thin sections from prospective neural ectoderm of post-gastrulating embryos reveals that neighboring cells (Fig. 1) are joined at their surfaces by a junctional complex (Fig. 2) consisting of a zonula occludens, zonula adherens, and macula adherens, as described by Farquhar and Palade (20). Numerous pentalaminar fusions (Fig. 2) of the outer leaflets of adjacent plasma membranes are common along the interface between the embryonic surface and the second junctional component, the zonula adherens. Although these points of fusion appear identical, only the most apical components impede the flow of tracers such as lanthanum, horseradish peroxidase, and K-pyroantimonate (Figs. 4, 5) regardless of how they are administered. Fig. 5 depicts the configuration of these apical membrane fusions as a belt or zonule, while basal fusions appear to be focal in character (see Friend and Gilula [22]). Freeze fracturing corroborates the existence of a tight, continuous zonula occludens and a more basal, loosely oriented, open network of ridges and complementary furrows (Fig. 6). Fig. 6 further illustrates the complementary nature of the ridges and furrows typical of an occluding zonule (12, 22, 30, 41, 73). Unlike the tight junctions of the pancreas (22), liver (30, 41), and mammary gland (61), freeze cleaving has failed to demonstrate gap junctions concealed within the confines of the amphibian zonulae occludentes. Ordinarily, the particles within tight junctional compartments exhibit a random orientation and lack a mirror image on the B face (Fig. 6, insets a and b).

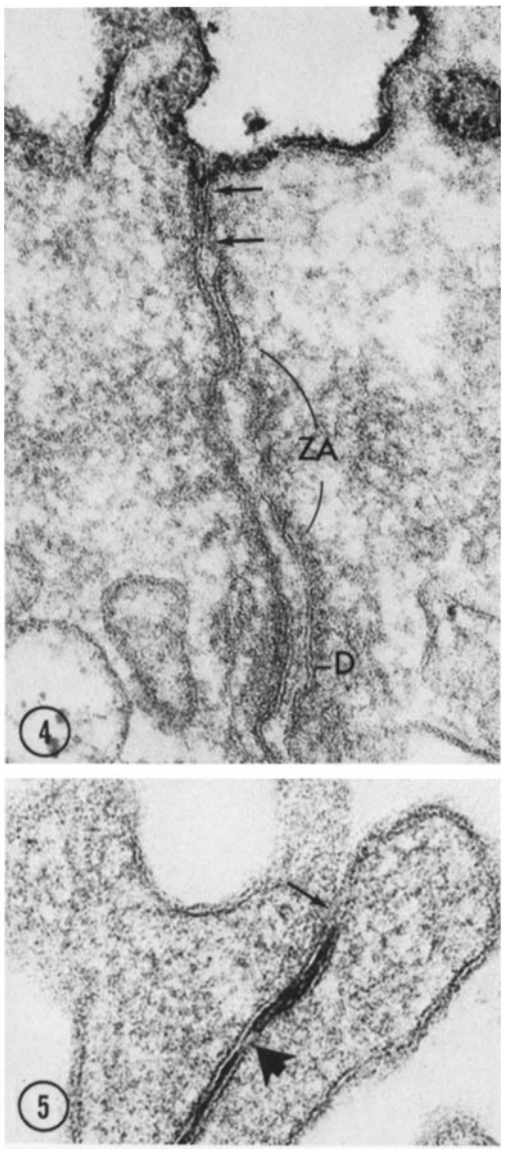

FIGURE 4 Neural plate embryo (stage 13) bathed in fixative containing 5% K-pyroantimonate. Apical membrane fusions of the *ZO* (arrows) prevent intercellular penetration of the tracer. The intercellular space between the intermediate junction (*ZA*) and the desmosome (*D*) is also free of tracer. × 116,000.

FIGURE 5 Colloidal-lanthanum-injected gastrocoel of a neural plate embryo (stage 13). Hydrostatic pressure has forced lanthanum to percolate between cells and around a focal tight junction (arrowhead), but the tracer was nonetheless halted at the most apical tight junction (arrow). × 152,000.

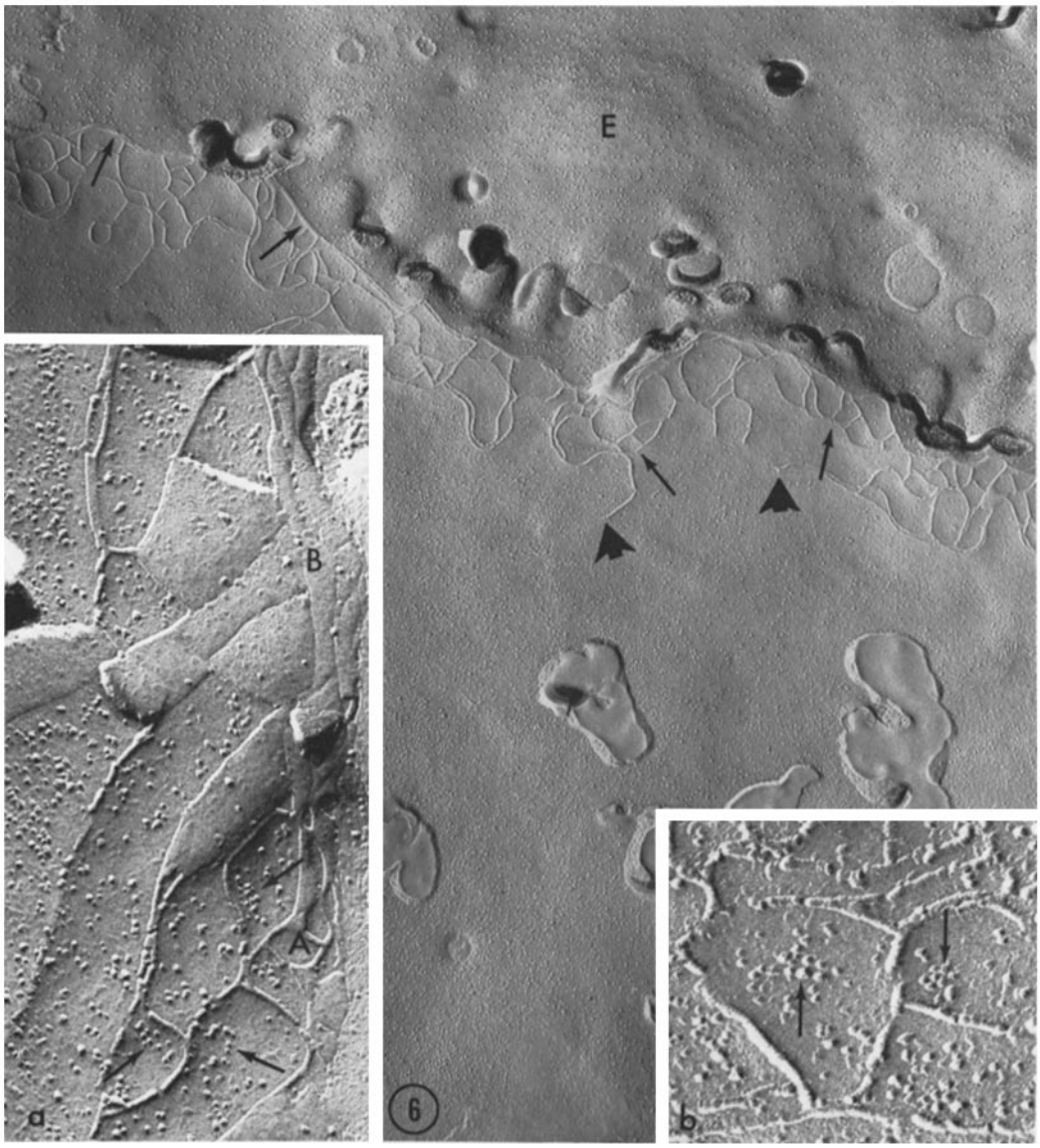

FIGURE 6 Freeze fracture illustrating the continuous ramifying mesh-work of 8.0-nm ridges which constitute the tight junction in preneurulating embryos (stage 12). Common features are the fusion of two ridges on the A face (arrows) and numerous disconnected ridges at the base of the junction (arrowheads). Note the ubiquity and uniformity of particle size (~120 Å) on the membrane facing the environment (*E*) as compared to the particle heterogeneity of adjacent cell membranes. Inset a: the complementary nature of A face ridges and B face furrows of the tight junction is shown here. Particles (80–100 Å) (arrows) are often found within the confines of junctional compartments. Inset b: small particle aggregates (arrows) in these compartments are depicted; however, the absence of complementary B face pits (inset a) indicates they are not gap junctions. × 32,400; inset a, × 92,000; inset b, × 130,000.

An intermediate junction (zonula adherens) of varying length lies directly below the occluding zonule (Figs. 2 and 4), apparently acting as an insertion site for microfilaments of the dense layer (see Schroeder [68]). Occasionally, punctate, pentalaminar fusions are interspersed within the adhering zonule (Figs. 2 and 4). Even though microfilaments seemingly eminate from the inner

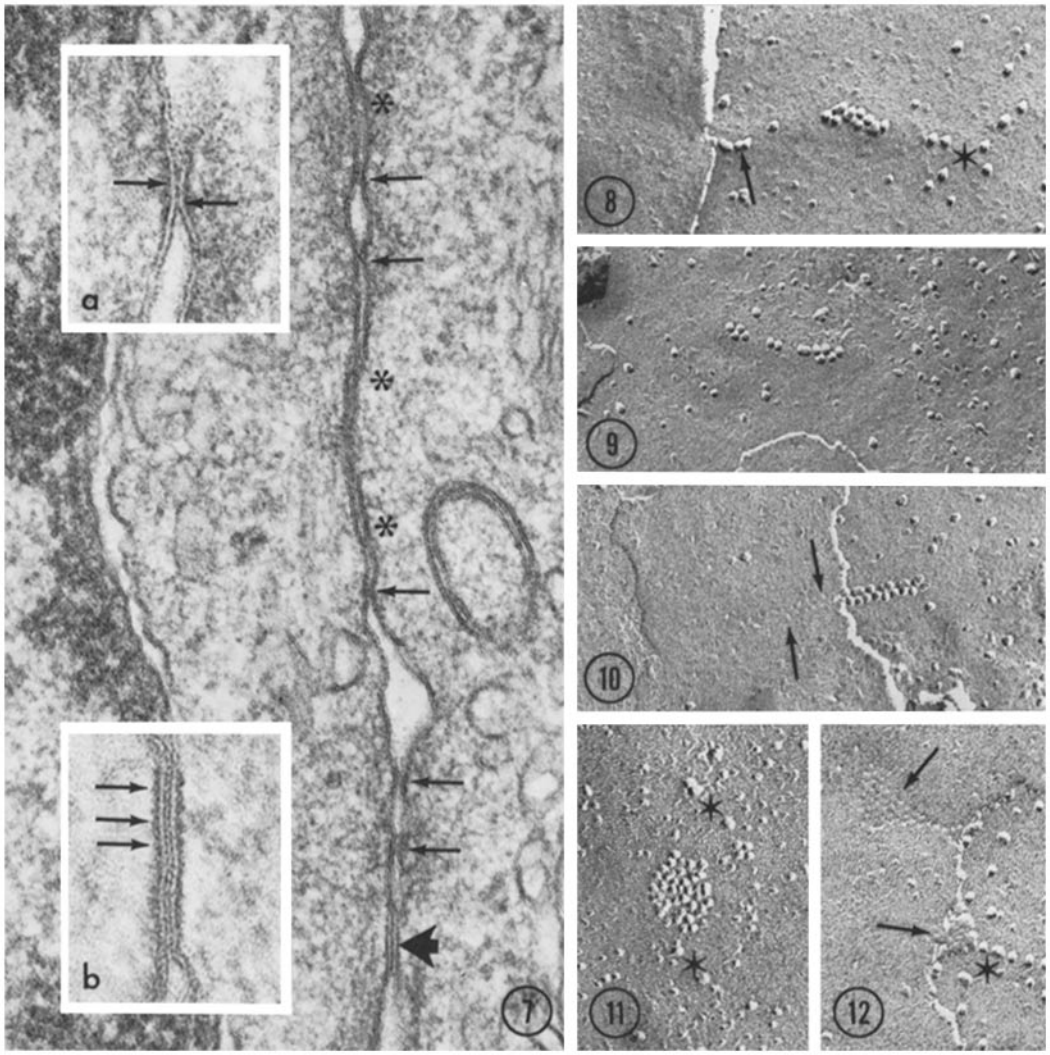

FIGURE 7 Well below the junctional complex (stage 13), membranes of adjacent presumptive ependymal cells approach within 2.0 to 4.0-nm (arrows), while other appositions are separated by an extracellular space varying up to 10 nm (asterisk) across. Discrete gap junctions (arrowhead), however, are rare. Inset a: one type of close membrane apposition with a 2.0-nm gap is illustrated here. Condensations of electron-dense material are associated with the cytoplasmic leaflets of this region (arrows). Inset b: a gap junction (~0.2 μm) with its 2.0 to 4.0-nm gap and periodic cytoplasmic densities (arrows) approximately 80 Å apart. × 85,500; inset a, × 180,000; inset b, × 187,000.

FIGURES 8–12 Freeze-cleaved replicas of these (see Fig. 7) membrane fusions reveal small amorphous patches (Figs. 8 and 9), beaded rows (Fig. 8, arrow), and doublet strings (Fig 10) of 85-Å particles (stage 12, 13). These membrane fusions appear to correlate to that illustrated in Fig. 7, inset a. Frequently, a B face image reveals the corresponding pits of these particle assemblies (Fig. 10, arrow; Fig. 12, arrow). Figs. 11 and 12: polygonal packing of macular gap junctions in both A (Fig. 11) and B (Fig. 12) faces. The stars denote the 10-nm particles that are frequently seen near such aggregates. Fig. 8, × 122,000; Fig. 9, × 112,000; Fig. 10, × 112,000; Fig. 11, × 120,000; Fig. 12, × 120,000.

leaflet of the plasma membrane, freeze fracturing discloses no unusual particle arrays in that region (see McNutt and Weinstein [47]).

The terminal element of the junctional complex in this embryonic epithelium is the macula adherens or desmosome (Figs. 2–4). Ordinarily, one diminutive desmosome, consisting of two dense plaques disposed parallel to the inner leaflets of the plasma membrane (Fig. 3), is evident just below the adhering zonule (Figs. 2, 4). Bundles of cytoplasmic tonofilaments converge on the inner aspect of each plaque, where they appear to terminate. An intercellular cleft 25.0 nm wide separates the outer plasmalemmal leaflets, which are bisected by a dense median line (21) (Fig. 3). Although other workers (10, 46, 47) have demonstrated a freeze-fracture correlate to the desmosomal plaque, such granular reliefs have not been observed in the replicas of this epithelium.

AMPHIBIAN GAP JUNCTIONS: Well below

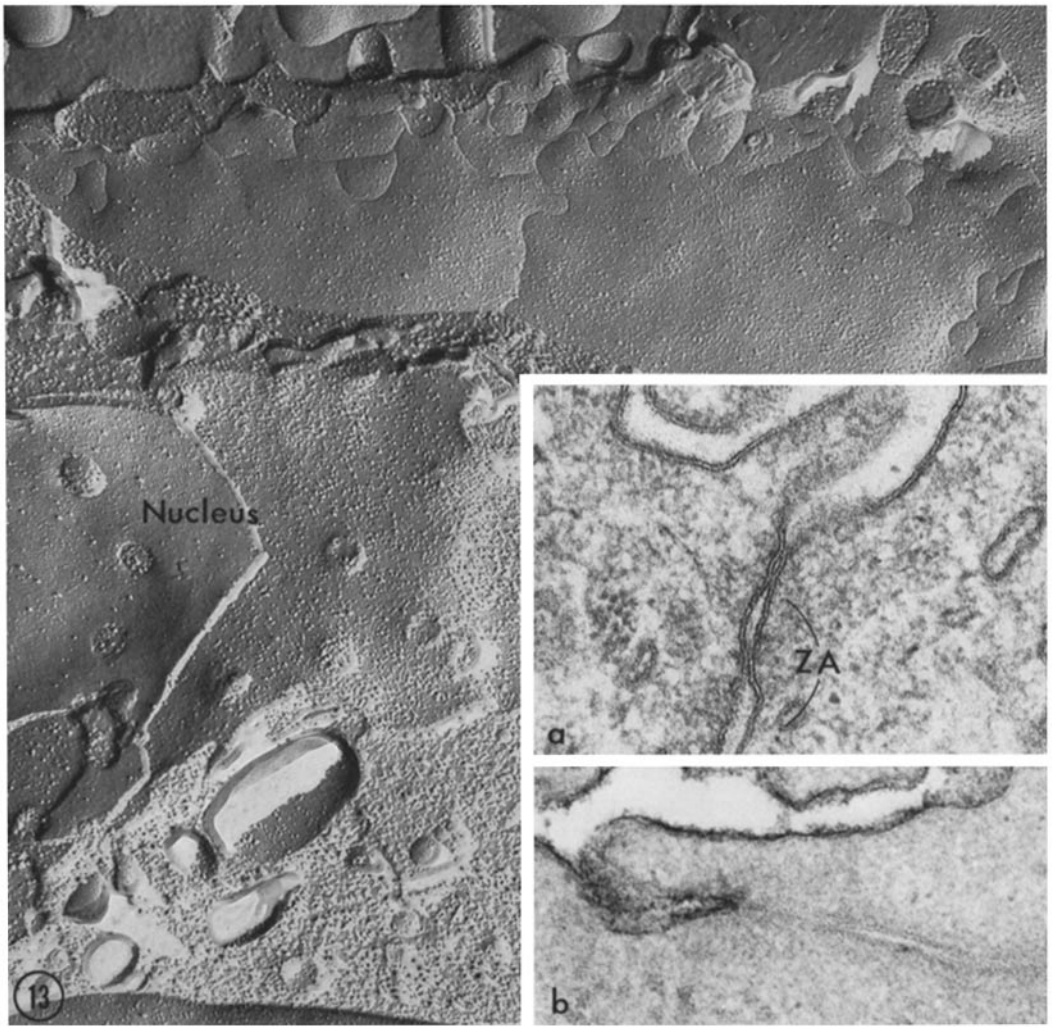

FIGURE 13 Occluding zonule at the base of an early neural groove (stage 13, 54.5 h of age). The tight junction has been transformed into a loose network of interconnected compartments. Fused ridges are no longer prevalent and no abluminal open ridges are apparent. Inset a: a distinct loss in punctuate fusions with corresponding development of the zonula adherens (*ZA*) is illustrated here. Generally, this modified tight junction impedes the flow of 5% K-pyroantimonate when embryos are bathed in this tracer (inset b). × 49,500; inset a, × 120,000; inset b, × 85,800.

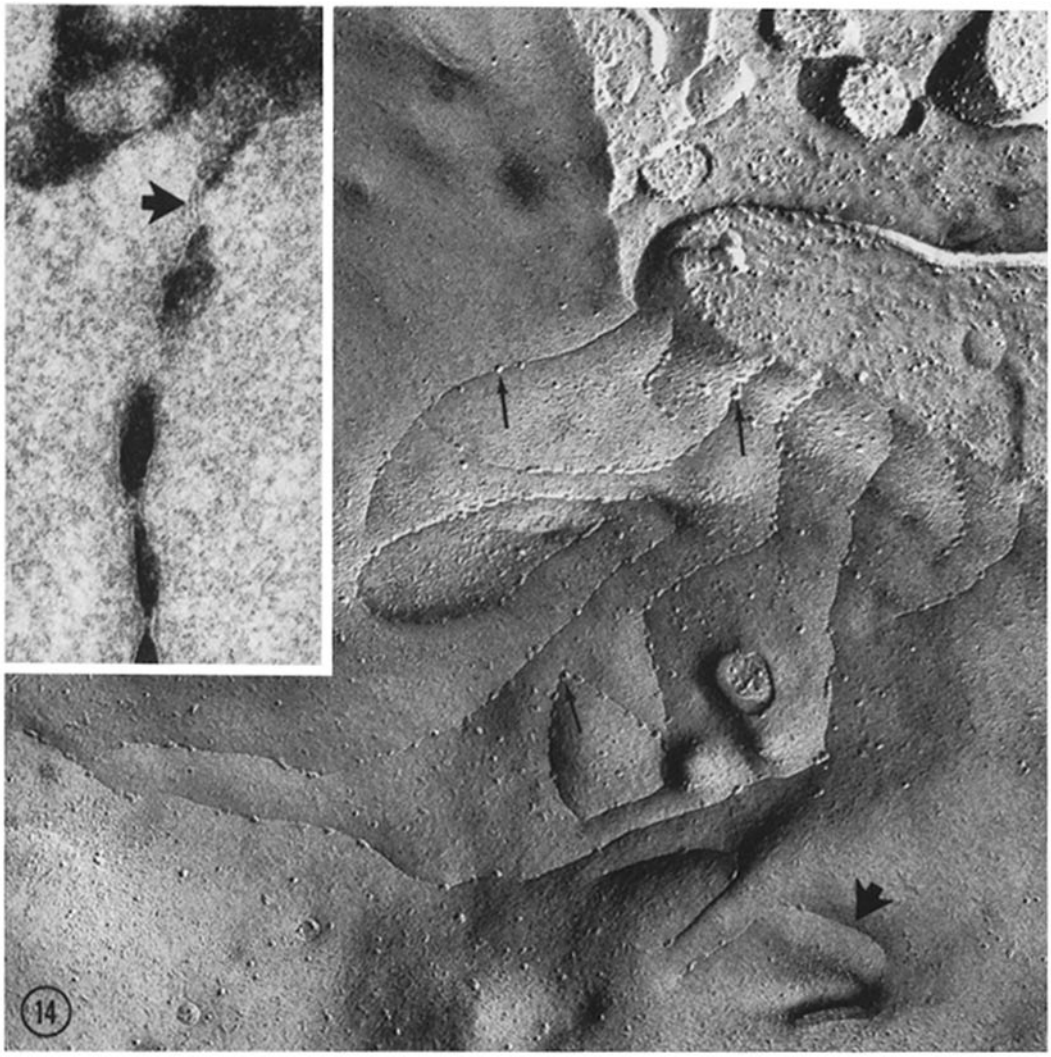

FIGURE 14 Tight junction midway in neurulation (stage 14). At this time, the junction fragments into widely dispersed domains in which the ridges (Fig. 15) and furrows (Fig. 14) are deployed parallel to the cell axis rather than in a belt. The junction is open-ended with little ramification or compartmentalization, and there are usually short, isolated fasciae occludentes (arrowhead) nearby. Frequently, 80 to 100-Å particles (arrows) are associated with the furrows, presumably torn away from the A face ridge during cleavage. In this section, lanthanum flows around such membrane fusions (arrowhead), demonstrating the porosity of this junction (inset). × 87,000; inset, × 116,000.

the junctional complex in embryonic epithelia, the lateral plasma membranes of future neuroepithelial cells exhibit a variety of "close" appositions varying from as much as 10 nm to as little as 2–4 nm apart (Fig. 7); however, only rarely are discrete gap junctions evident in thin sections (Fig. 7, inset b). When such close membrane associations are examined after freeze cleaving, small aggregates of particles are visible (Figs. 8–12). Morphologically, their configuration varies from distinct macules (Figs. 11 and 12) to longitudinal strands (Fig. 10); but generally they are seen as small, amorphous patches of particles (Figs. 8 and 9). As few as 4 and as many as 30 particles make up these "gap-like" junctions. A distribution of particle sizes further reveals that two classes of par-

ticles are prevalent in many of the arrays. One measures 8–9 nm and is found in the small, closely packed aggregates (Figs. 8–12, 27). The other particle is approximately 10 nm in diameter and is prominent in the relatively smooth regions surrounding the aggregates (Figs. 8, 12, 27). Occasionally B face profiles possess complementary pits, a common feature of the gap junction (Figs. 10 and 12). These depressions or pits seen on the B face are usually 3.0–4.0 nm in diameter, and in macular gap junctions contain regions of hexagonal packing (Fig. 12).

Cell Junctions in Neurulating Embryos

FATE OF THE ZONULA OCCLUDENS: As the neural groove deepens (see Schroeder [68]), a marked change occurs in the configuration and extent of the occluding zonule. Thin sections taken from the base of the neural groove reveal a paucity of punctate, pentalaminar membrane fusions when compared to those of preneurulating embryos (Fig. 13, inset a). Similarly, once prominent desmosomes are no longer present in these flask-shaped cells. Such fine structural alterations are directly reflected by the appearance of the tight junction in freeze-cleaved replicas (Fig. 13). The continuous, parallel belt of ridges and complementary furrows commonly found earlier in embryogenesis has been transformed into a loosely knit zonule composed of a network of interlocking compartments (compare Fig. 13 with Fig. 6). The former clearly distinguished belt of tightly interdigitating ridges

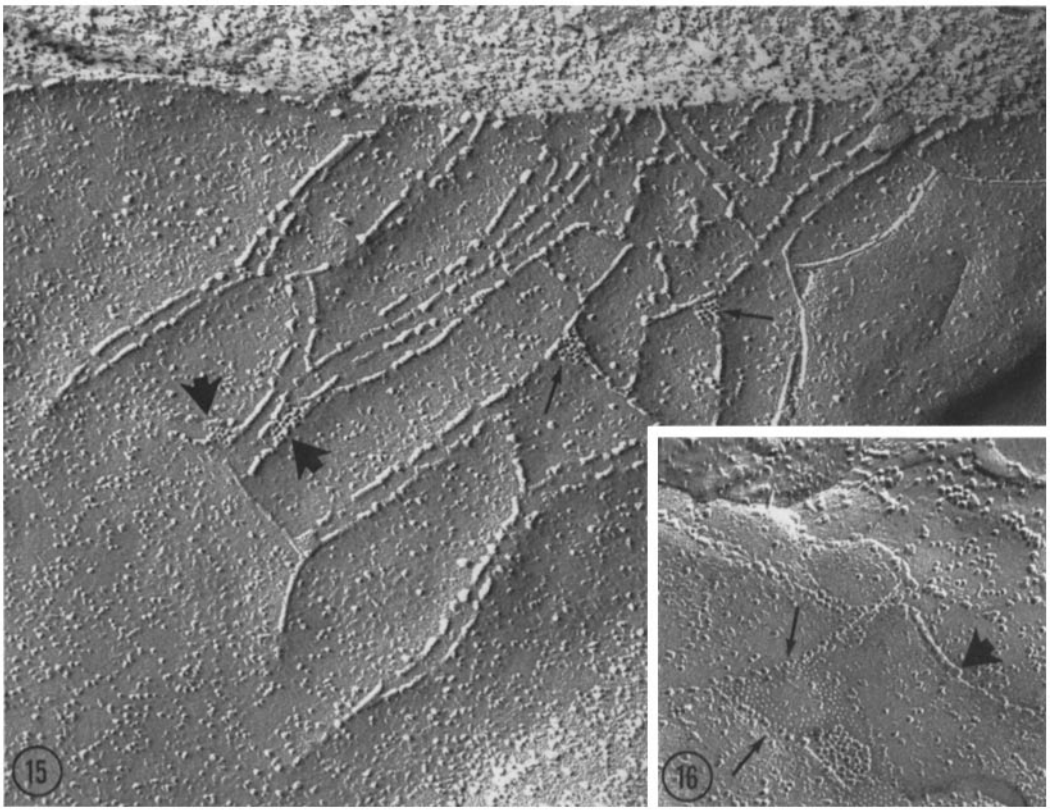

FIGURE 15 Another tight junctional domain (stage 14). Here, numerous 85-Å particles accumulate against many of those ridges which intersect (arrows) or closely approach (arrowhead) one another. × 65,000.

FIGURE 16 Particle arrays in tight junctional domains (stage 14). Polygonal packing and complementary depressions in the B face indicate the gap junctional nature of the aggregates. Tight junction ridges encasing a gap junction often take on a beaded appearance (arrows). The particles measure about 90 Å and are quite similar to gap particles. Other ridges in the domain are beaded or particulate interspersed with smoothly contoured ridges (arrowhead), suggesting junctional disassembly. × 78,000.

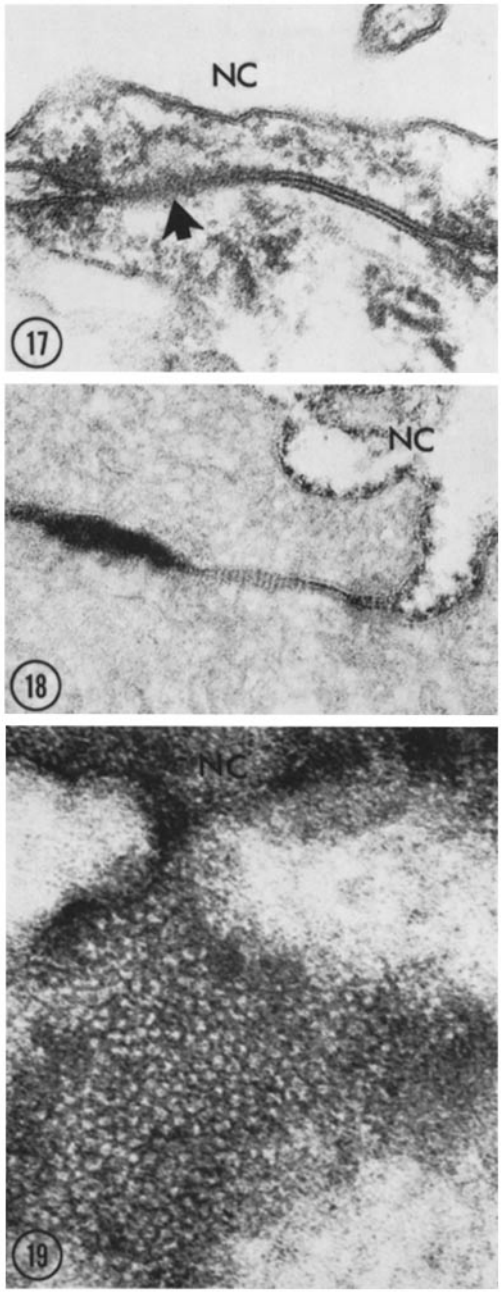

FIGURES 17–19 Thin sections through neural tube embryos (stages 15, 16). Adjacent cells are joined apically by gap junctions. Fig. 17 is a routine preparation simultaneously depicting a transverse and an oblique (arrowhead) section through a gap junction. Ruthenium red (Fig. 18) and lanthanum (Fig. 19) further delineate the substructure of the gap junction. Fig. 18 illustrates a transverse section of a gap junction. Fig. 19 reveals the *en face* distribution of gap junction subunits. *NC*, neural canal. Fig. 17, × 92,000; Fig. 18, × 101,500; Fig. 19, × 210,000.

(Fig. 6) and the characteristic doublet and fused ridges (Fig. 6, inset a) are no longer prevalent. Although the zonula occludens is much less complex, it still succeeds in excluding a variety of tracers (Fig. 13, inset b).

With progressive excavation of the neural groove and simultaneous elevation of the surrounding neural folds (68), the occluding zonule fragments into solitary domains (Figs. 14 and 15). In freeze-fractured specimens, these tight junctional domains generally extend perpendicular to rather than parallel to the embryonic surface, without much ramification or compartmentalization (Figs. 14 and 15). Isolated ridges or furrows (fasciae occludentes) are also visible nearby (Figs. 14 and 15). Moreover, tracers readily pass around pentalaminar fusions and through this junction, emphasizing their porosity (Fig. 14, inset). Such images of strands and furrows no longer correspond to true zonulae occludentes.

All evidence of organized regions of complementary ridges and furrows vanishes with the convergence and subsequent closure of the neural folds (Fig. 20). Fasciae occludentes are rarely seen, and then they appear as random, disoriented ridges. Freeze fracturing further reveals that former tight junctional ridges and some gap junctions are closely associated (Fig. 21). This interrelationship will be discussed more specifically in the next section.

ASSEMBLY OF GAP JUNCTIONS IN ASSOCIATION WITH TIGHT JUNCTIONAL REMNANTS: With the fragmentation of the zonulae occludentes into domains, numerous 8.5-nm particles apparently aggregate in many regions where tight junctional ridges intersect or closely appose (Figs. 15, 16). These particles abut against the intersecting ridges, and in some instances appear polygonally packed (Fig. 15). In other areas, where large openings exist within the former tight junction, the particles are also predominantly associated with a ridge (Fig. 15). Freeze-cleaved replicas illustrating the B face to advantage display the complementary 3.0 to 4.0-nm depressions characteristic of the gap junction (Fig. 16). Heavy metal tracers percolate around and in between these particles, further delineating the structure of the gap junction (Figs. 18 and 19).

Portions of the encircling ridges often have a distinctive beaded texture (Fig. 16). In such regions, 8 to 9-nm particles constitute what apparently was formerly a ridge, while in other sites they are interspersed among smoothly contoured components of a ridge. Frequently, the beaded rows blend into a ridge, in apparent continuity (Fig. 16).

With neural fold closure, the past prominent occluding zonule is replaced by widely distributed gap junctions (Figs. 17 and 20). Only the random, disoriented ridges of the fasciae occludentes and the gap-associated ridges (Fig. 21) remain as evidence of earlier tight junctions. The fasciae occludentes appear to be unrelated to the disposition of ependymal cells, while the 8.0-nm gap junction-associated ridges, though rare, seem linked to particles in the gap junctional periphery (Fig. 21). Despite their unknown origin, these elements may represent remnants of the old tight junction which once partially encompassed the developing gap junction and simply retained their continuity with the outer particles.

ASSEMBLY OF BASAL GAP JUNCTIONS: In postgastrulating embryos (stages 12 and 13), the lateral cell membranes of prospective neuroepithelial cells contain small concentrations of 8.5-nm particles, some exhibiting polygonal packing in freeze-fracture replicas (Figs. 11 and 12) and a 2.0

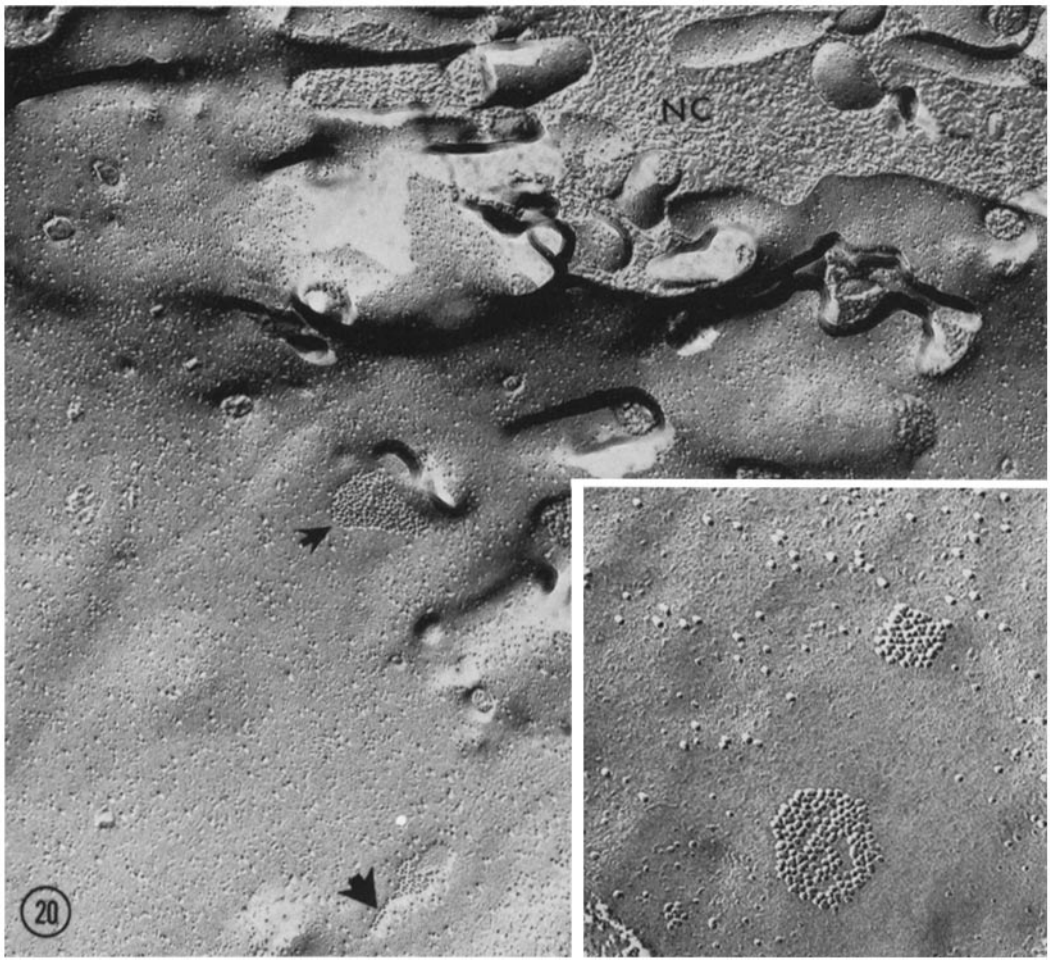

FIGURE 20 Freeze fracture demonstrating absence of tight junctions and the presence of gap junctions in neural tube embryos (stage 16). These junctions are widely distributed (arrowheads), and basal junctions occasionally possess tails. The particles of gap junctions are packed in two ways: Smaller junctions have closely packed, polygonally arranged particles; most larger ones have particle-free aisles. *NC*, neural canal. × 49,500; inset, × 111,000.

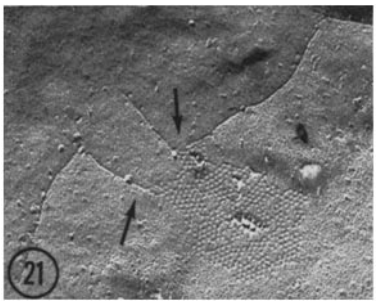

FIGURE 21 Tight junctional ridges in continuity (arrows) with apical gap junctions (stage 15). In this occasional phenomenon, the ridges apparently emanate from gap particles in junctional peripheries and probably are remnants of the occluding zonules. × 73,500.

to 4.0-nm gap in thin section (Fig. 7, inset b). As longitudinal infolding of the neural plate commences (stage 14), long streams of 10-nm particles appear within the plasma membrane (Figs. 22, 23). These intramembranous particles are commonly separated by some distance (Figs. 22 and 23), yet occasionally appear as chains (Fig. 22), and are generally polarized by a small company of particles at one end of the stream (Figs. 22 and 23). Under favorable circumstances, this particulate array resides in an otherwise particle-free membranous region, giving the area the impression of a halo (Fig. 23). Although these regions are more difficult to visualize in B face profiles, complementary depressions of these linear arrangements of particles are prevalent (Figs. 24 and 25).

Subsequently, particles of the array apparently merge with the periphery of the aggregate, where they seem to become reorganized and polygonally packed into a gap junction. Sometimes the particles form a tail composed of two closely proximate rows of granules (Figs. 26 and 27). That this "doublet tail" is part of the gap junction is verified by the complementary nature of its B face pits (Fig. 26). The tails then seem to be incorporated into the periphery of the junction, giving it a macular configuration (Fig. 20, inset). The packing of particles in the macular gap junction assumes two distinct forms: smaller gap junctions usually exhibit compact, polygonal packing, whereas larger ones possess particle-free regions within the central area (Fig. 20, inset). It is not known whether they represent gap junctions of functionally different types; however, we did not visualize all the variations in gap particle disposition described by Staehelin (71) and Peracchia (54, 55).

DISCUSSION

Although the visualization of gap junctions has been enhanced by utilizing heavy metal tracers and stains (11, 22, 24, 30, 32, 33, 34, 63), negative staining (4, 30, 55, 81), and freeze fracturing (12, 22, 30, 46, 47, 55, 61, 74, 81), these studies have contributed little in describing their construction in developing or mature tissues. While some gap junctions are diminutive and macular (22, 47, 64, 65, 66), others exhibit a diversity of contours: some are long, particulate chains such as those in the outer plexiform layer of the retina (62), and still others are small, amorphous, particle aggregates similar to those of normal and transformed fibroblasts (28, 58, 64). In liver, adrenals, and smooth muscle (22, 30), they appear as large, variegated maculae. Staehelin (71) observed the coexistence of three separate configurations of gap junctions between adjacent rat intestinal epithelial cells. These distinctions are based on the variations in size, spacing, and arrangement of their constituent particles (71). Peracchia (54, 55) has also illustrated gap junction heterogeneity in the crayfish segmental axon. Both Staehelin and Peracchia intimate that such structural diversity dictates the existence of *functionally* differing gap junctions.

Pinto da Silva and Gilula (58) speculated that such distinctive particle arrays, especially the smaller maculae and beeded rows (see Friend and Gilula [22] and Revel et al. [65]), may represent one aspect of gap junctional membrane differentiation. Yee's (80) description of gap junctional behavior after partial hepatectomy tends to support this. Here, large gap junctions vanish, only to reappear 37–40 h after surgery as minute maculae, subsequently proliferating into the large junctions characteristic of liver (80). A slight variation in this theme has been described by Johnson and Preus (37) who report that as early as 5 min after the reaggregation of Novikoff hepatoma cells has begun, small clusters of 100-Å particles appear on relatively flat, particle-free areas of the A face of the cell membrane. By 30 min the number of particles has increased and some of them have formed arrays resembling gap junctions. Johnson (personal communication) believes that these large particles represent some form of gap junction precursor. Such small particle aggregates may act as focal nucleation sites (25) which could polarize gap junctional differentiation (25, 58, 80).

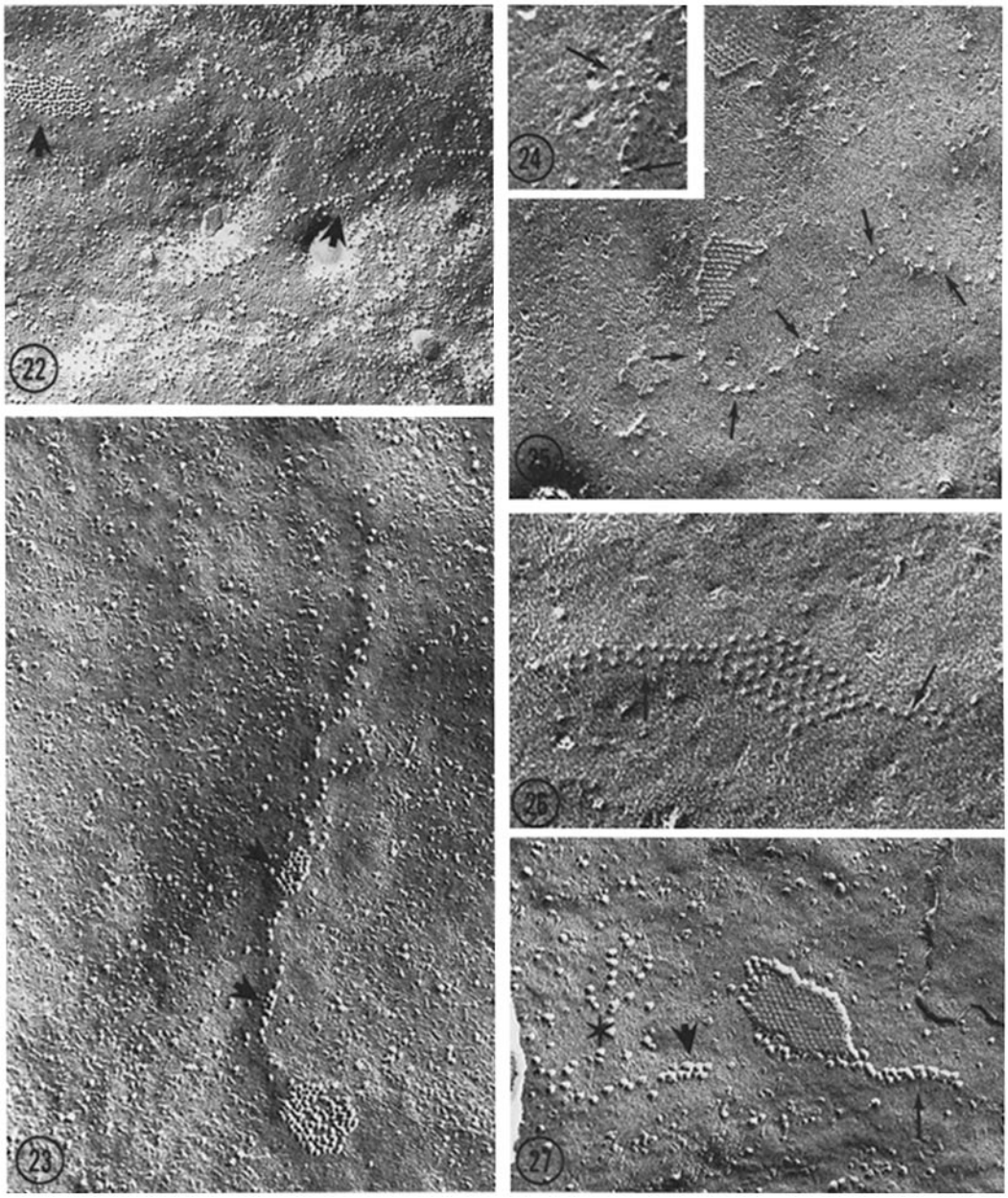

FIGURES 22–27 Stages of basal gap junction assembly. Fig. 22 illustrates the 100-Å particulate chains, and Fig. 23 depicts the streams. These arrays apparently terminate in small aggregates of 85-Å particles (arrowheads). A particle-free halo encompassing a series of such streams is prominent in Fig. 23. In B face profiles, the streams are linear, arrayed in complementary 2 to 3-nm depressions (arrows) corresponding in location to that of particles on the A face of the replica (Figs. 24 and 25). As the gap junction takes form (Figs. 26 and 27), particulate streams diminish and are replaced by a single or double row of particles emanating as a tail (arrows). B face replicas reveal a complementary image of the tail, intimating their gaplike nature (Fig. 26). Fig. 27 illustrates both A and B face components of the junction. Nearby, another gap junction appears to be in the early stages of construction. Note the small aggregate of 8 to 9-nm particles (arrowhead) and the neighboring cluster of 100-Å granules (star). Fig. 22, × 60,000; Fig. 23, × 95,700; Fig. 24, × 285,000; Fig. 25, × 75,000; Fig. 26, × 220,000; Fig. 27, × 91,000.

Alterations in the Apical Junctional Complex

With progressive excavation of the neural groove, the zonulae occludentes open and then fragment into isolated dominions. In many areas where tight junction ridges converge or intersect, numerous 8.5-nm particles accrue (Fig. 15), frequently appearing polygonally packed. B face profiles illustrate complementary depressions that characterize the arrays as gap junctions (Fig. 16).

Probably tight junctional ridges represent a rather rigid, well-anchored structure within the lipid matrix of the plasma membrane (70), and it is plausible that such intersecting or closely apposed ridges may participate prominently in assembling gap junctions. Whether gap particles originate *de novo* and are then inserted into the membrane, or are formed by the convergence of preexistent intramembranous particles, intersecting ridges may provide a scaffolding to channel particles to a point of intersection where they can intermingle and form a polygonal lattice. Moreover, such a framework might insure the proper register of particles in one membrane with those in the adjacent membrane to create a functional gap junction. The common presence of tight junctional elements in close contact with gap particles (Fig. 21) suggests that strong intramolecular forces exist between components of both. That gap junctions are intercalated within the confines of other occluding zonules further emphasizes the probability of an intimate relationship between the structural components of the two elements (22, 30, 31, 41, 47, 61).

The ultimate fate of the fragmented occluding zonule is unknown (65); however, several observations imply that tight junction remnants may either dedifferentiate or be removed *in toto* from the cell membrane. Evidence of intermittent, beaded rows of particles within the contour of a tight junction ridge (Fig. 16; see Friend and Gilula [22]) suggests that the ridge may break up into its constituent subunits during neurulation. Further documentation is, however, essential before this hypothesis can be elaborated upon. Alternatively, nonfunctional tight junctions may be eliminated by internalizing the membrane upon which they reside (65, 72). A recent report of isolated tight junction ridges localized within lysosome-like organelles indicates that junctional dissolution may take place through endocytosis of junctional membrane (72). Moreover, after dissociating cells with trypsin, Overton (51) has demonstrated that "half"-desmosomes are also rapidly incorporated into similar intracellular vacuoles, further implicating an endocytic mode.

Differentiation of Basal Gap Junctions

Well beneath the amphibian junctional complex, the genesis of gap junctions is asynchronous, occurring throughout neurulation.[1] Here, however, no clearly identifiable structure augments their assembly. Instead, our initial observations of late gastrulae reveal several unique membranous areas which contain small aggregates of 8 to 9-nm particles encompassed by larger (10 nm) granules. As neurulation commences the number of large particles increases, creating long, linear arrays occasionally interrupted by small aggregates which assume the form of gap junctions (Figs. 22–25). Conceivably, these particle-aggregates act as nucleation sites similar to the furrows described by Gilula (25) which organize the formation of the septate junction in sea urchin embryos. It is likely that the differentiating gap junction enlarges as its prospective particles (100-Å granules) blend with the periphery of the aggregate. A recent observation of Johnson and Preus (37) also indicates that a large, 100-Å particle may denote a precursor to the smaller, 80-Å subunit of the Novikoff hepatoma gap junction (35). The fusion of particles into a doublet tail (Figs. 26 and 27) may characterize an intermediate stage in reorganizing the gap particles into a macular configuration.

Gap Junction Formation within the Plasma Membrane

Convincing evidence exists that freeze fracturing provides extensive *en face* views of a cleavage plane through the center of the hydrocarbon tails which compose the lipid bilayers of biological membranes (8, 9, 13, 57). This unique fracture creates two complementary membrane components: a cytoplasmic half termed fracture face A, and its extracellular homologue, fracture face B (12, 57, 76, 79). Numerous randomly distributed particles reside in these fracture faces (particles in the A face outnumber those in the B face), which probably represent proteins that traverse the hydrophobic core of the membrane (19, 56, 60). In

[1] As a consequence of the asynchrony accompanying gap junction formation, the steps in their construction must, out of necessity, reflect the authors' bias.

contrast, nonparticulate regions of each face may reflect the continuous lipid matrix (14, 70). Moreover, etching experiments on human erythrocyte ghosts indicate that these particles possess ABO antigens (57, 59), influenza virus binding sites, and phytohemagglutinin receptors (77). Consequently, they must include the glycoproteins and/or glycolipids. And in view of Goodenough's data on the isolation and partial characterization of mouse liver gap junctions (30, 31), it would seem that gap particles depicted in freeze-cleaved replicas are probably lipoprotein complexes.

If these studies accurately reflect the macromolecular nature of intramembranous particles (in particular, gap particles), the events associated with their assembly into a supramolecular architecture like that of the gap junction should be demonstrable. The recent visualization of translational mobility of antigens on the surface of virus-fused heterokaryons (23), lymphocyte capping (40), lateral diffusion of antimuscle plasma membrane antibody (18), and rosette formation during mucocyst secretion (67), all suggest that membrane fluidity (70) affords the mechanism for the aggregation of particles into gap junctions. Since the gap junction is probably the site of electrotonic coupling and intercellular transport of larger molecules (5, 66), the particles must be exposed to an environment that is successively hydrophilic, then hydrophobic, and ultimately hydrophilic again. Hence, they may differ from other intramembranous particles and may also possess a mutual affinity. Experiments involving pH and proteolysis in erythrocyte ghosts imply that the sites of intramembranous particles (19, 56, 60) and colloidal iron hydroxide (49) are partly dependent on electrostatic charge. The action of phospholipase C, however, intimates that hydrophobic interactions between membrane phospholipids and the particles are also essential to stabilization (49). At present, which of these factors are critical in assembling gap particles into a functional junction remains to be elucidated.

We gratefully acknowledge the technical prowess of Ms. Yvonne Jacques and Ms. Irene Rudolf, and are indebted to Miss Rosamond Michael for her peerless editing and preparation of this manuscript. One of us (Robert S. Decker) wishes to express his thanks to Mrs. Madelon Smith for typing the revised version of this manuscript.

This study was supported by United States Public Health Service Fellowship No. 5-F02-GM-36168-01 and -02 to Dr. Decker, and National Institutes of Health Grant HD-06895 to Dr. Friend.

Recieved for publication 13 August 1973, and in revised form 19 February 1974.

REFERENCES

1. ABERCROMBIE, M. 1970. *In Vitro.* **6**:128.
2. ASADA, Y., and M. V. L. BENNETT. 1971. *J. Cell Biol.* **49**:159.
3. AZARNIA, R., W. MICHALKE, and W. R. LOWENSTEIN. 1972. *J. Membrane Biol.* **10**:247.
4. BENEDETTI, E. L., and P. EMMELOT. 1968. *J. Cell Biol.* **38**:15.
5. BENNETT, M. V. L. 1973. *Fed. Proc.* **32**:65.
6. BENNETT, M. V. L., and J. P. TRINKAUS. 1970. *J. Cell Biol.* **44**:592.
7. BENNETT, M. V. L., M. E. SPIRA, and G. D. PAPPAS. 1972. *Dev. Biol.* **29**:419.
8. BRANTON, D. 1966. *Proc. Natl. Acad. Sci. U. S. A.* **55**:1048.
9. BRANTON, D., and D. W. DEAMER. 1972. Membrane Structure (Monograph II: E-1). Protoplasmalogia (Wien). Springer-Verlag, New York.
10. BREATHNACH, A. S., C. STOLINSKI, and M. GROSS. 1972. *Micron.* **3**:278.
11. BRIGHTMAN, M. W., and T. S. REESE. 1969. *J. Cell Biol.* **40**:648.
12. CHALCROFT, J. P., and S. BULLIVANT. 1970. *J. Cell Biol.* **47**:49.
13. DEAMER, D. W., and D. BRANTON. 1967. *Science (Wash. D. C.).* **158**:655.
14. DEAMER, D. W., R. LEONARD, A. TARDIEU, and D. BRANTON. 1970. *Biochim. Biophys. Acta.* **219**:47.
15. DEHAAN, R. L., and H. G. SACHS. 1972. *Curr. Top. Dev. Biol.* **7**:193.
16. DEWEY, M. M., and L. BARR. 1970. *Current Topics in Membranes and Transport.* **1**:1.
17. DOOLIN, P. F., and W. J. BIRGE. 1969. *J. Comp. Neurol.* **136**:253.
18. EDIDIN, M., and D. FAMBROUGH. 1973. *J. Cell Biol.* **57**:27.
19. ENGSTROM, L. H. 1970. Ph.D. Dissertation. University of California, Berkeley, California.
20. FARQUHAR, M. G., and G. E. PALADE. 1963. *J. Cell Biol.* **17**:375.
21. FARQUHAR, M. G., and G. E. PALADE. 1965. *J. Cell Biol.* **26**:263.
22. FRIEND, D. S., and N. B. GILULA. 1972. *J. Cell Biol.* **53**:758.
23. FRYE, L. D., and M. EDIDIN. 1970. *J. Cell Sci.* **7**:319.
24. FURSHPHAN, E. J., and D. N. POTTER. 1968. *Curr. Top. Dev. Biol.* **3**:95.
25. GILULA, N. B. 1972. *J. Cell Biol.* **55** (2, Pt. 2):86 a.
26. GILULA, N. B., D. BRANTON, and P. SATIR. 1970. *Proc. Natl. Acad. Sci. U. S. A.* **67**:213.

27. GILULA, N. B., and P. SATIR. 1971. *J. Cell Biol.* **51**:869.
28. GILULA, N. B., O. R. REEVES, and A. STEINBACH. 1972. *Nature (Lond.).* **235**:262.
29. GOODENOUGH, D. A., S. ITO, and J.-P. REVEL. 1968. *Biol. Bull. (Woods Hole).* **135**:420.
30. GOODENOUGH, D. A., and J.-P. REVEL. 1970. *J. Cell Biol.* **45**:272.
31. GOODENOUGH, D. A., and W. STOECKENIUS. 1972. *J. Cell Biol.* **54**:646.
32. HAND, A. R., and S. GOBEL. 1972. *J. Cell Biol.* **52**:397.
33. HUDSPETH, A. J., and J.-P. REVEL. 1971. *J. Cell Biol.* **50**:92.
34. ITO, S., and W. R. LOWENSTEIN. 1969. *Dev. Biol.* **19**:228.
35. JOHNSON, R. G. 1972. *J. Cell Biol.* **55**(2, Pt. 2): 126a.
36. JOHNSON, R. G., and J. D. SHERIDAN. 1971. *Science (Wash. D. C.).* **174**:717.
37. JOHNSON, R. G., and D. PREUS. 1973. *J. Cell Biol.* **59**(2, Pt. 2):158 a.
38. JOSEPH, T., C. SLACK, and R. P. GOULD. 1973. *J. Embryol. Exp. Morphol.* **29**:681.
39. KALT, M. R., and B. TANDLER. 1971. *J. Ultrastruct. Res.* **36**:633.
40. KARNOVSKY, M. J., and E. R. UNANUE. 1973. *Fed. Proc.* **32**:55.
41. KREUTZIGER, G. O. 1968. Proceedings of the 26th Annual Electron Microscopist Society of America. **26**:234.
42. LENTZ, T. L., and J. P. TRINKAUS. 1971. *J. Cell Biol.* **48**:455.
43. LOWENSTEIN, W. R. 1973. *Fed. Proc.* **32**:60.
44. LUFT, J. H. 1964. *J. Cell Biol.* **23**:54A.
45. MARTZ, E., and M. S. STEINBERG. 1972. *J. Cell Physiol.* **79**:189.
46. MCNUTT, N. S., and R. S. WEINSTEIN. 1970. *J. Cell Biol.* **47**:666.
47. MCNUTT, N. S., and R. S. WEINSTEIN. 1973. *Prog. Biophys. Mol. Biol.* **26**:45.
48. MOOR, H., and K. MUHLETHALER. 1963. *J. Cell Biol.* **17**:609.
49. NICOLSON, G. L. 1973. *J. Cell Biol.* **57**:373.
50. OSCHMAN, J. L., and M. J. BERRIDGE. 1970. *Tissue Cell.* **2**:281.
51. OVERTON, J. 1968. *J. Exp. Zool.* **168**:203.
52. PAPPAS, G. D., Y. ASADA, and M. V. L. BENNETT. 1971. *J. Cell Biol.* **49**:173.
53. PAYTON, B. W., M. V. L. BENNETT, and G. D. PAPPAS. 1969. *Science (Wash. D. C.).* **166**:1641.
54. PERACCHIA, C. 1973. *J. Cell Biol.* **57**:54.
55. PERACCHIA, C. 1973. *J. Cell Biol.* **57**:66.
56. PINTO DA SILVA, P. 1972. *J. Cell Biol.* **53**:777.
57. PINTO DA SILVA, P., and D. BRANTON. 1970. *J. Cell Biol.* **45**:598.
58. PINTO DA SILVA, P., and N. B. GILULA. 1972. *Exp. Cell Res.* **71**:393.
59. PINTO DA SILVA, P., D. BRANTON, and S. D. DOUGLAS. 1971. *Nature (Lond.).* **232**:194.
60. PINTO DA SILVA, P., P. S. MOSS, and H. H. FUDENBERG. 1973. *Exp. Cell Res.* **81**:127.
61. PITELKA, D. R., S. T. HAMAMOTO, J. G. DUAFALA, and M. K. NEMANIC. 1973. *J. Cell Biol.* **56**:797.
62. RAVIOLA, E., and N. B. GILULA. 1973. *Proc. Natl. Acad. Sci. U. S. A.* **70**:1677.
63. REVEL, J.-P., and M. J. KARNOVSKY. 1967. *J. Cell Biol.* **33**:C7.
64. REVEL, J.-P., A. G. YEE, and A. J. HUDSPETH. 1971. *Proc. Natl. Acad. Sci. U. S. A.* **68**:2924.
65. REVEL, J.-P., P. YIP, and L. L. CHANG. 1973. *Dev. Biol.* **35**:302.
66. SATIR, P., and N. B. GILULA. 1973. *Annu. Rev. Entomol.* **18**:143.
67. SATIR, B., C. SCHOOLEY, and P. SATIR. 1973. *J. Cell Biol.* **56**:153.
68. SCHROEDER, T. E. 1970. *J. Embryol. Exp. Morphol.* **23**:427.
69. SHUMWAY, W. 1942. *Anat. Rec.* **83**:309.
70. SINGER, S. J., and G. L. NICOLSON. 1972. *Science (Wash. D. C.).* **175**:720.
71. STAEHELIN, L. A. 1972. *Proc. Natl. Acad. Sci. U.S.A.* **69**:1318.
72. STAEHELIN, L. A. 1973. *J. Cell Sci.* **13**:763.
73. STAEHELIN, L. A., T. M. MUKHERJEE, and A. W. WILLIAMS. 1969. *Protoplasma.* **67**:165.
74. STEERE, R. L., and J. R. SOMMER. 1972. *J. Microsc. (Paris).* **15**:205.
75. STOKER, M. 1967. *Curr. Top. Dev. Biol.* **2**:107.
76. TILLACK, T. W., and V. T. MARCHESI. 1970. *J. Cell Biol.* **45**:649.
77. TILLACK, T. W., R. E. SCOTT, and V. T. MARCHESI, 1972. *J. Exp. Med.* **135**:1209.
78. TRELSTAD, R. L., E. D. HAY, and J.-P. REVEL. 1967. *Dev. Biol.* **16**:78.
79. WEHRLI, E. K., K. MUHLETHALER, and H. MOOR. 1970. *Exp. Cell Res.* **59**:336.
80. YEE, A. G. 1972. *J. Cell Biol.* **55**(2, Pt. 2):294 a.
81. ZAMPIGHI, G., and J. D. ROBERTSON. 1973. *J. Cell Biol.* **56**:92.